A Phase-Field Model Coupled with Lattice Kinetics Solver for Modeling Crystal Growth in Furnaces

Guang Lin[1,*], Jie Bao[2], Zhijie Xu[1], Alexandre M. Tartakovsky[1] and Charles H. Henager Jr.[3]

[1] *Computational Mathematics Group, Pacific Northwest National Laboratory, Richland, WA 99352 USA.*
[2] *Fluid and Computational Engineering Group, Northwest National Laboratory, Richland, WA 99352 USA.*
[3] *Engineering Mechanics and Structure Materials Group, Northwest National Laboratory, Richland, WA 99352 USA.*

Abstract. In this study, we present a new numerical model for crystal growth in a vertical solidification system. This model takes into account the buoyancy induced convective flow and its effect on the crystal growth process. The evolution of the crystal growth interface is simulated using the phase-field method. A semi-implicit lattice kinetics solver based on the Boltzmann equation is employed to model the unsteady incompressible flow. This model is used to investigate the effect of furnace operational conditions on crystal growth interface profiles and growth velocities. For a simple case of macroscopic radial growth, the phase-field model is validated against an analytical solution. The numerical simulations reveal that for a certain set of temperature boundary conditions, the heat transport in the melt near the phase interface is diffusion dominant and advection is suppressed.

1 Introduction

Numerical simulations of crystal growth from the melt in vertical gradient furnaces [1, 2] has attracted significant attention due to the importance of crystals in a number of medical imaging applications and for radiation detection [3–5].

---

*Corresponding author. *Email addresses:* `guang.lin@pnnl.gov` (G. Lin), `jie.bao@pnnl.gov` (J. Bao), `zhijie.xu@pnnl.gov` (Z. Xu), `alexandre.tartakovsky@pnnl.gov` (A. M. Tartakovsky), `chuck.henager@pnnl.gov` (C. H. Henager Jr.)

Vertical growth methods include both high-pressure and ambient pressure methods with recent advances in ambient pressure methods coming to the fore [5]. Ambient pressure methods offer reduce experimental complexity and have been shown to produce large single crystal volumes with properties as good or better than high-pressure methods, thus, there has been a shift towards low-pressure methods using vertical gradient furnaces and sealed ampoule growth [5]. However, material uniformity, property homogeneity, and crystal defects remain difficult problems to solve for certain systems grown in this manner, such as Cd-Zn-Te (CZT). Modeling and simulation techniques have been advanced as a route to understanding the solidification process in complex systems and are thought to provide a more systematic method for determining optimal growth conditions and improved materials.

Recent advances in computer models for growth processes in the vertical gradient furnace have been useful in understanding the general effects of furnace operating conditions on the growth of crystals [6]. As such, computer models became a valuable tool in the furnace design and optimization of operating conditions [7–11]. At the same time, most existing models use a simplistic description of crystal/melt interface and its dynamic. Furthermore, in these models it was assumed that the latent heat dissipates without disturbing the continuity of the heat fluxes at the interface. This approach fails to account for the effects of crystal anisotropy and solidification kinetics, which may be important in the simulations of crystal dendritic growth or lateral overgrowth [12,13]. Here, we have developed a phase-field based model to simulate crystal growth in the vertical gradient furnace. The model takes into account the effects of anisotropy in kinetic and interfacial free energy coefficients as well as the effect of front curvature on crystal growth. The model was used to study the effects of operating and boundary conditions on crystal growth in a prototypical vertical gradient furnace.

The phase-field method has become a standard tool to tackle free-boundary problems and simulate interfacial pattern formation phenomena in solidification and other systems [14–16]. The phase-field method avoids explicit front tracking by replacing sharp interfaces with spatial-smoothly diffused boundaries between bulk phases. Thus, the phase-field method is suitable for simulating time-dependent free-boundary problems, especially when complex geometries are present. In a phase-field model, an order parameter, phase-field variable ψ is introduced to smoothly vary from one value in the liquid region to another one in the solid region. This method is not only used to simulate solidification but is also able to track solid-solid phase transformations and is suitable for general microstructural evolution problems. Thus, solidification and subsequent microstructural coarsening during high-temperature furnace processing can all be addressed within the same simulation framework.

The main difficulty for simulating the fluid field in the liquid region is the time-dependent growth interface between the liquid and solid phase. Hence a semi-implicit lattice kinetics model [17] based on the Boltzmann equation method [18–21]is used for solving the fluid flow instead of using the traditional computational fluid dynamics (CFD) method based on solving Navier-Stokes equations. One of the advantages of the

lattice method is dealing with complicated or moving solid boundaries. Besides that, it is well known that the original lattice Boltzmann model(LBM) shows high efficiency in parallel computation, and the lattice kinetics method [22]was designed to eliminate the need to store and transmit the elements of the particle velocity distribution function, which was believed to theoretically reduce the data transmit between compute nodes for massive parallel computation [17, 23]. The semi-implicit lattice kinetics method is modified from the original lattice kinetics method, and increases the stability for large time steps [17]. In the following section we present the differential equations that govern the melt convection, heat conduction and solidification process in the vertical gradient furnace. In Section 3, we present the numerical model and steps for the solution of the governing equations. In Section 4, we discuss the results of numerical simulations for different operational conditions.

2   Governing equations

Melt flow and crystal growth in a vertical gradient furnace can be described by a Boltzmann equation with the simple BGK collision operator and energy conservation equations:

$$\frac{\partial f}{\partial t} + \vec{u} \cdot \nabla f = \frac{f - f^{eq}}{Y}, \qquad\qquad x \in \Omega_l, \tag{2.1a}$$

$$\frac{\partial T}{\partial t} + u\frac{\partial T}{\partial x} + v\frac{\partial T}{\partial y} = \frac{K^l}{\rho^l C_p^l}\nabla^2 T, \quad x \in \Omega_l, \tag{2.1b}$$

$$\frac{\partial T}{\partial t} = \frac{K^s}{\rho^s C_p^s}\nabla^2 T, \qquad\qquad x \in \Omega_s, \tag{2.1c}$$

$$\rho L V_i = K_s \partial_n T_s - K_l \partial_n T_l, \qquad\quad x \in \Gamma, \tag{2.1d}$$

$$T_i - T_m = -\frac{\vartheta}{\rho L}K T_m - \beta V_i, \qquad\quad x \in \Gamma, \tag{2.1e}$$

where Ω_l is the domain occupied by the liquid phase (melt), Ω_s is the domain occupied by the solid phase (crystal), $\Gamma = \Omega_s \bigcap \Omega_l$ is the interface between crystal and melt, β_T is thermal expansion, ϑ is the surface tension, L is the latent heat, β is the kinetic coefficient, u and v are components of velocity $\vec{u}$ in the x and y directions (y is in the vertical direction), P is pressure, ρ^l, ρ^s, K^l, K^s, C_p^l and C_p^s represent the density, thermal conductivity and specific heat capacity of the solution and solid, T_i and T_m are interface temperature and melting temperature respectively. V_i is normal interfacial velocity. f is the particle distribution function (PDF), and represents the probability of finding particles at position $\vec{x}$ with velocity $\vec{u}$ at time t. f^{eq} is the equilibrium Maxwell distribution [24]. Y is a linear relaxation parameter. More details and numerical methods for the Boltzmann equation will be introduced in following sections. Eqs. (2.1) are subject to the following boundary conditions:

At the top of the crucible wall: The no-slip, no-flow boundary conditions are employed, (i.e., $u=0$ and $v=0$) and the thermal boundary condition is:

$$\frac{\partial T}{\partial n} = 0. \tag{2.2}$$

At the vertical crucible wall: The no-slip boundary conditions are employed at the vertical walls between the surrounding crucible and the liquid. Thus, $u=0$ and $v=0$. The thermal boundary conditions for the vertical crucible walls are:

$$-\kappa_s \frac{\partial T}{\partial n} = h(T - T_f(y)), \tag{2.3}$$

where h is the heat transfer coefficient, $T_f(y)$ is the ambient temperature inside the furnace along the quartz ampoule walls, and can be calculated by Eq. (2.4) [25]

$$T_f(y) = \frac{1}{2} \left\{ T_c + T_h + (T_h - T_c) \tanh \left[\left(\frac{dT_f(0)}{dy} \right) \frac{(y - y_i)}{(T_h - T_c)} \right] \right\}, \tag{2.4}$$

where T_c is cold-end temperature, T_h is hot-end temperature, and $\frac{dT_f(0)}{dy}$ is the maximum axial derivative of the ampoule-wall temperature profile. y_i is the approximate position of the melt-solid interface. Generally, there are two main types of setup for applying the temperature profile $T_f(y)$ on the ampoule wall. The first one is choosing a reference frame fixed with the imposed temperature distribution on a stationary wall [26]. In this frame, the ampoule and solidified material move axially at velocity $-U_{pull}$, equal in magnitude and opposite in sign to the velocity of the phase interface in a frame moving with the ampoule. We call this setup fixed temperature profile setup, and y_i is a fixed value. The second one is letting the frame move with the moving ampoule, so the melt-solid interface grows at velocity U_{pull}. We call this setup time-dependent temperature profile setup, and $y_i = y_{i0} + U_{pull}t$. The first setup causes less computation cost on updating the computation mesh, so it is favorable for the interface tracking method. The model in this paper does not need to update the computation mesh when interface is moving, so the computation cost for our model is the same for these two kinds of wall temperature profile setup.

3 Numerical methods

Eqs. (2.1) constitute a (highly non-linear) free-boundary problem due to the presence of moving solid-liquid interface Γ. The phase-field method [15] was used to reduce the free-boundary problem to a system of coupled Boltzmann, energy, and phase-field equations. In the phase-field equation, the state variable ψ takes a value of 1 in the solid phase

(crystal) and -1 in the liquid phase (melt)

$$\frac{\partial f}{\partial t} + \vec{u} \cdot \nabla f = \frac{f - f^{eq}}{Y} + \widetilde{F}, \qquad x \in \Omega_l, \tag{3.1a}$$

$$\frac{\partial T}{\partial t} + u \frac{\partial T}{\partial x} + v \frac{\partial T}{\partial y} = \alpha_l \nabla^2 T + S_\psi, \quad x \in \Omega_l, \tag{3.1b}$$

$$\frac{\partial T}{\partial t} = \alpha_s \nabla^2 T, \qquad x \in \Omega_s, \tag{3.1c}$$

and

$$\tau \frac{\partial \psi}{\partial t} = \left[\psi - \lambda \frac{C_p}{L} (T - T_m)(1 - \psi^2) \right] (1 - \psi^2)$$
$$+ W^2 \nabla^2 \psi + 2W \frac{\partial \psi}{\partial x} \frac{\partial W}{\partial x} + 2W \frac{\partial \psi}{\partial y} \frac{\partial W}{\partial y}$$
$$+ \frac{\partial}{\partial x} \left\{ [(\partial_x \psi)^2 + (\partial_y \psi)^2] W \frac{\partial W}{\partial(\partial_x \psi)} \right\}$$
$$+ \frac{\partial}{\partial y} \left\{ [(\partial_x \psi)^2 + (\partial_y \psi)^2] W \frac{\partial W}{\partial(\partial_y \psi)} \right\}, \quad x \in \Omega,$$

where $\Omega = \Omega_l \bigcup \Omega_s$. $W(n) = W_o a_s(n)^2$, W_o is the dimensionless interface thickness, $\tau(n) = \tau_o a_s(n)^2$ is the dimensionless characteristic time of atom attachment, and, for crystals with four-fold symmetry, $a_s(n) = (1 - 3\epsilon_4)[1 + \epsilon'(n_x^4 + n_y^4)]$. In the sharp interface limit, the phase-field parameters W_o, τ_o and λ are related to the physical parameters d_o and β via $d_o = a_1 \frac{W}{\lambda}$ and $\beta(n) = \frac{a_1 \tau(n)}{\lambda W(n)}[1 - a_2 \frac{W(n)}{D\tau(n)}]$, where $a_1 = 0.8839$ and $a_2 = 0.6267$ [15]. The vanishing interface kinetics ($\beta = 0$) limit can be achieved by setting $\lambda = \frac{1}{a_2} \frac{\alpha \tau_o}{W_o^2}$. In the energy equations, α_l and α_s are the thermal diffusivity of liquid and solid phases respectively. The model is only valid in the symmetric conductivity limit, so $\alpha_l = \alpha_s$ [15, 27]. S_ψ is a heat source term caused by the phase transition, and it varies in different kinds of wall temperature profile setups. For the first case, fixed wall temperature profile setup, $S_\psi = \frac{L}{2C_p} \frac{\partial \psi}{\partial y} U_{pull}$. For the second setup, time-dependent temperature profile setup, $S_\psi = \frac{L}{2C_p} \frac{\partial \psi}{\partial t}$.

A semi-implicit lattice method [17] is employed to solve the Boltzmann equation for the fluid field. After being discretized in momentum, spatial, and time spaces, the particle distribution function f becomes a finite set of displacement vectors connecting each lattice site to adjacent sites. Fig. 1 shows the lattice directions for the commonly used 2-dimensional D2Q9 lattice. The discrete external forcing term ($\widetilde{F}$) can be calculated in the lattice scheme by [28]:

$$\widetilde{F}_i = \left(1 - \frac{1}{2Y}\right) w_i \left(\frac{\vec{e}_i - \vec{u}}{c_s^2} + \frac{\vec{e}_i \cdot \vec{u}}{c_s^4} \vec{e}_i\right) \cdot \vec{F}, \tag{3.2}$$

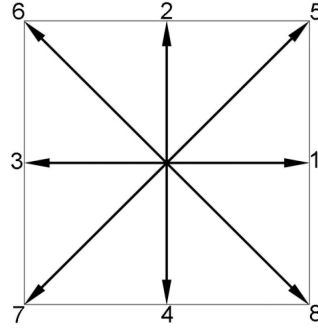where $\vec{F}$ is the external force. In the semi-implicit lattice method, the pressure and veloc-

Figure 1: D2Q9 lattice.

ity can be updated by the following equations:

$$p^{n+1} = \frac{p^n + \eta \left(\sum_{i=1}^{N} f_{i,\rho}^{\vec{x}-\vec{e_i}} \right)^{n+1} - \eta \frac{3}{2} w_0 \frac{\rho \vec{u} \cdot \vec{u}}{c^2}}{1 + \frac{\eta}{c_s^2}(1 - w_0)}, \tag{3.3}$$

$$\vec{u}^{n+1} = \frac{(\rho \vec{u})^n + \left(\sum_{i=1}^{N} \vec{e_i} f_{i,\vec{u}}^{\vec{x}-\vec{e_i}} \right)^{n+1} + \vec{S_0}}{\rho + \rho \frac{6\nu}{c^2 \Delta t} + S_1}, \tag{3.4}$$

where η is the derivative of pressure with respect to density. The superscript n indicates values at the beginning of the time step, and the $n+1$ stands for estimated values at the end of the time step. N is the total number of lattice directions excluding the stationary 0 direction. ν is the fluid viscosity, $c = \Delta x / \Delta t$ is the reference lattice speed, and $c_s^2 = c^2/3$ is the lattice sound speed [29]. w_i is the weight coefficient, for a D2Q9 system, $w_0 = 4/9$, $w_{1-4} = 1/9$ and $w_{5-8} = 1/36$ [30]. $\vec{e_i}$ is the unit vector. $\vec{S_0}$ is momentum source terms. The buoyancy force can be applied in the term $\vec{S_0}$

$$\vec{S_0} = \vec{g} \rho \Delta t \beta_T (T - T_0), \tag{3.5}$$

where T_0 is a reference temperature, $\vec{g}$ is gravity, and β_T is thermal expansion. S_1 is a mass source term, which can be used to emulate Darcy resistance in a porous medium [17]. In Eqs. (3.3) and (3.4), $f_{i,\rho}^{\vec{x}-\vec{e_i}}$ and $f_{i,\vec{u}}^{\vec{x}-\vec{e_i}}$ represents the particle probability distribution arriving from the neighboring lattice site in the $-\vec{e_i}$ direction, and they can be calculated by

$$f_{i,\vec{u}} = w_i \left[\frac{p}{c_s^2} + \frac{6\nu\rho}{c^2 \Delta t} \frac{3\vec{e_i} \cdot \vec{u}}{c^2} + \rho \left(\frac{9(\vec{e_i} \cdot \vec{u})^2}{2c^4} - \frac{3\vec{u} \cdot \vec{u}}{2c^2} \right) \right], \tag{3.6}$$

$$f_{i,\rho} = w_i \left[\frac{p}{c_s^2} + \rho \frac{3\vec{e_i} \cdot \vec{u}}{c^2} + \rho \left(\frac{9(\vec{e_i} \cdot \vec{u})^2}{2c^4} - \frac{3\vec{u} \cdot \vec{u}}{2c^2} \right) \right]. \tag{3.7}$$

One of the lattice method's strengths is dealing with boundary conditions. It is very easy to apply a complicated or moving solid wall boundary condition, like phase interface, to lattice method for flow simulation. Halfway bounce back treatment is a widely

used simple boundary condition for lattice methods [31–33], which requires the solid boundary is in the middle of two lattices, and offers second order accuracy. For practical problems, especially for curved boundary, the solid boundary cannot always locate at the middle of two lattices perfectly. Hence, for more accurate and smoother velocity field near curved boundary without requiring high mesh resolution, Filipova and Hänel (FH) proposed a curved wall boundary condition [34], which later was improved by Mei, Luo and Shyy (MLS). Bao, Yuan and Schaefer further refined this technique to solve the mass conserving problem when body force is applied on the fluid field [35], and this boundary condition treatment was used in the proposed model. For a moving boundary, such as the phase interface, the momentum source from moving wall can be incorporated into distribution function as $2w_i\rho\frac{3}{c^2}\vec{e}_i\vec{u}_w$, where $\vec{u}_w$ is wall speed. This implicit lattice kinetics method has the advantage of being stable at larger time steps but requiring an iterative solution. The detailed iteration method and steps were introduced in Rector's work [17].

A finite difference method with uniform mesh size was used to solve the system of governing partial equations for energy and phase-field. To sufficiently resolve the phase-field function, the grid size should satisfy the condition $W_o \leq 2.5\Delta$ [15], and $W_o = 2.5\Delta$ is used in the tests that are presented in the following sections. The remaining phase-field parameters were chosen as follows:

$$\lambda = a_1\frac{W_o}{d_o}, \qquad \tau_o = \frac{a_2 W_o^2 \lambda}{\alpha}. \tag{3.8}$$

The main steps for crystal growth simulation are: (1) Calculate velocity profile in lattice kinetics scheme with known temperature from last time step to estimate the buoyancy force; (2) Calculate temperature profile with the known velocity profile from step 1; (3) Calculate the phase-field with the known temperature profile from step 2; (4) Update the position of the phase interface, and construct the liquid and solid domain; (5) Go to next time step. We use the program ParaFlow for the solving fluid flow and temperature field and combine with a finite difference solver for solving the phase-field. ParaFlow is a large-scale parallel computational fluid dynamics program based on the semi-implicit lattice method [23].

4   Results and discussion

4.1   Phase-field model validation

To test the phase-field model, the growth of the circular seed due to solidification in the absence of melt was simulated numerically and resulting temperature profiles and the radius of the seed as a function of time are compared with analytical solutions [36]. We consider the case in which the interface separating solid and liquid phases is at radius $r = R(t)$, the region $r > R$ contains liquid and the region $r < R$ contains solid. Initially the interface is located at $r = a$ and the temperature of the liquid phase is equal to the melting temperature T_m. For $t > 0$ the surface $r = a$ is maintained at the $T = T_{in}$

Physical parameter	Values
Specific heat C_p $(Jkg^{-1}K^{-1})$	380
Thermal conductivity k $(Wm^{-1}K^{-1})$	42.8
Mass density ρ (kgm^{-3})	5633
Thermal expansion β_T (K^{-1})	1.2×10^{-4}
Viscosity μ $(kgm^{-1}s^{-1})$	7.35×10^{-4}
Melting temperature (K)	1211.4 k
Latent heat L (Jkg^{-1})	4.65×10^{5}
Surface tension ϑ (Nm^{-1})	0.554

$(T_{in} < T_m)$ and the temperature at $r = \infty$ is equal to the melting temperature. Table 1 lists the physical properties of the benchmark solidification problem (thermal constants ρ, c_p, k, κ were assumed to be the same for liquid and solid phases). In the phase-field simulations, a $[0,0.1m]\times[0,0.1m]$ domain was used, and Fig. 2 shows the simulation domain configurations. Different grid sizes ($\triangle$)are used for testing the results' convergence for different grid sizes and interface thicknesses (W_0). The tested grid sizes are $\triangle = 0.1/100$, $0.1/300$, $0.1/600$, $0.1/1000$, and $0.1/3000[m]$, and the corresponding interface thicknesses are $W_0 = 2118d_0$, $706d_0$, $353d_0$, $211d_0$, and $71d_0$ ($W_0 = 2.5\triangle$ is used). The phase-field parameters were chosen based on Eq. (3.8). This choice of parameters yields $\beta = 0$. For most of the materials, the capillary length is on the order of $10^{-6}[m]$. For the interface with a radius of curvature greater than $0.0015[m]$ and $\beta = 0$, the interfacial temperature is approximately equal to the melting temperature. The analytical solution for the solidification problem with $T = T_m$ at the interface is given by [36]:

$$2R^2 ln(R/a) - R^2 + a^2 = 4KT_m t/L\rho, \tag{4.1}$$

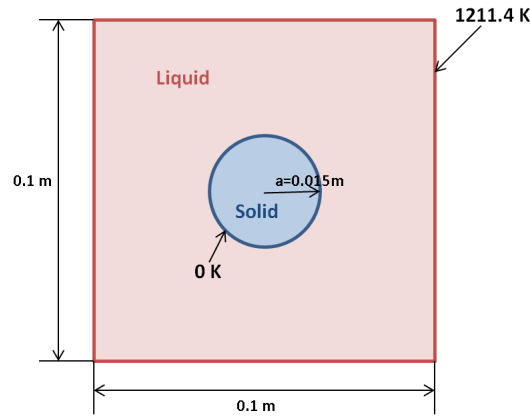

Figure 2: Sketch of the simulation domain for the model validation.

and

$$T = \frac{T_m \ln(r/a)}{\ln(R/a)}, \quad a < r < R, \qquad (4.2a)$$

$$T = T_m, \qquad\qquad r > R. \qquad (4.2b)$$

Fig. 3 compares results obtained from the phase-field model with the analytical solutions. Fig. 3 (a) presents the radius of the solidification interface as a function of time for different W_0. For $W_0 < 706 d_0$, the results can match the analytical solution perfectly. Fig. 3 (b) describes the thermal field as a function of radius at different times obtained from the analytical solutions and our phase-field model for $\triangle = 0.1/600[m]$ ($W_0 = 353 d_0$). Good agreement is observed between the numerical results and the analytical solutions in Fig. 3, confirming a high accuracy of the phase-field model for the parameters shown in Table 1. Similar parameters were used in crystal growth simulations presented in the following section.
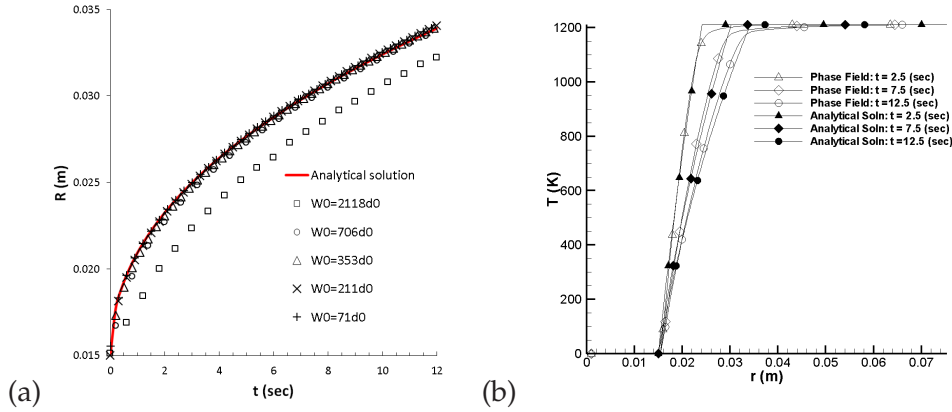

Figure 3: (a) Radius of the solidification interface as a function of time and (b) thermal field as a function of radius at different times for a solidification problem with cylindrical symmetry.

4.2 Simulations of the crystal growth in vertical gradient furnaces

This section presents the results of numerical simulations of the crystal growth in the vertical gradient furnaces. The crucible in the simulations is $0.016[m]$ wide, $0.32[m]$ tall, and the size of lattice $\Delta = 1 \times 10^{-4}[m]$. The heat transfer coefficient, $h = 150.0[W\,m^{-2}K^{-1}]$, is used in the boundary condition shown in Eq. (2.3). The solidification of the melt in the furnace is controlled by the temperature profile $T_f(y)$ which is shown in Eq. (2.4). Hot-end temperature $T_h = 1223[K]$, and cold-end temperature $T_c = 1154[K]$. Fig. 4 shows the sketch of initial setup of the solidification system and temperature profile on the vertical wall. For initial conditions, $\vec{u} = 0$, $\psi = -1$ in liquid, $\psi = 1$ in solid, and the initial temperature is calculated from Eq. (2.4). The Reynolds number of the system is about 1.7×10^4,
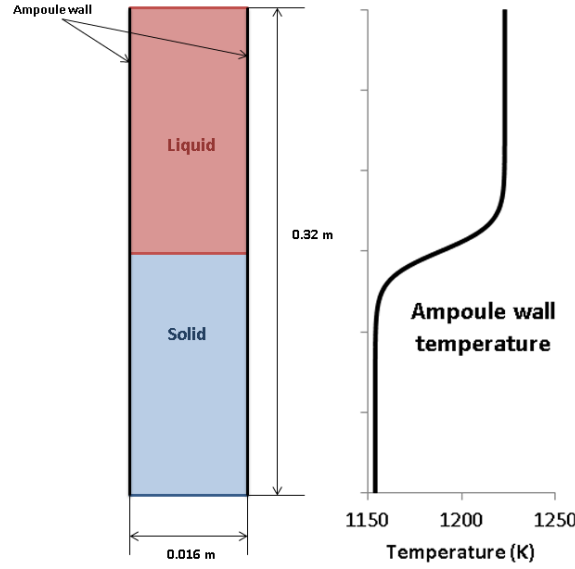
Figure 4: Sketch of the vertical solidification system and temperature profile on the vertical wall.

so the $k-\epsilon$ turbulence model was incorporated with the proposed semi-implicit lattice kinetics model through Filippova's approach [37].

Tables 1 and 2 provide the physical properties and non-dimensionless numbers used in the simulations. Fig. 5 shows the contour of temperature, streamline, and phase interface in a vertical crystal growth system with pulling speed $U_{pull}=6.668\times10^{-6}[ms^{-1}]$. The color of the streamline represents the magnitude of velocity $U=\sqrt{u^2+v^2}$. The crystal growth reaches steady state around 200 seconds. Fig. 6 shows the contour of temperature, streamline, and phase interface in a furnace with pulling speed $U_{pull}=1.3336\times10^{-5}[ms^{-1}]$. The maximum magnitude of velocity in the weak circulation near the phase interface is $5.5\times10^{-4}[ms^{-1}]$ for the slower pulling speed case ($U_{pull}=6.668\times10^{-6}[ms^{-1}]$), and $9.8\times10^{-4}[ms^{-1}]$ for the faster pulling speed case ($U_{pull}=1.3336\times10^{-5}[ms^{-1}]$). It is clear that the faster pulling speed causes stronger circulation near the phase interface, which may decrease the quality of the crystal during the growth process. Hence, it should be balanced between crystal quality and productivity. Fig. 7 shows the comparison of phase interface shapes between different pulling speeds in a vertical crystal growth system. Higher pulling speed causes bigger curvature of the phase interface. The

Table 2: Non-dimensionless numbers and their characteristic values used in the simulations of crystal growth in the vertical gradient furnace.

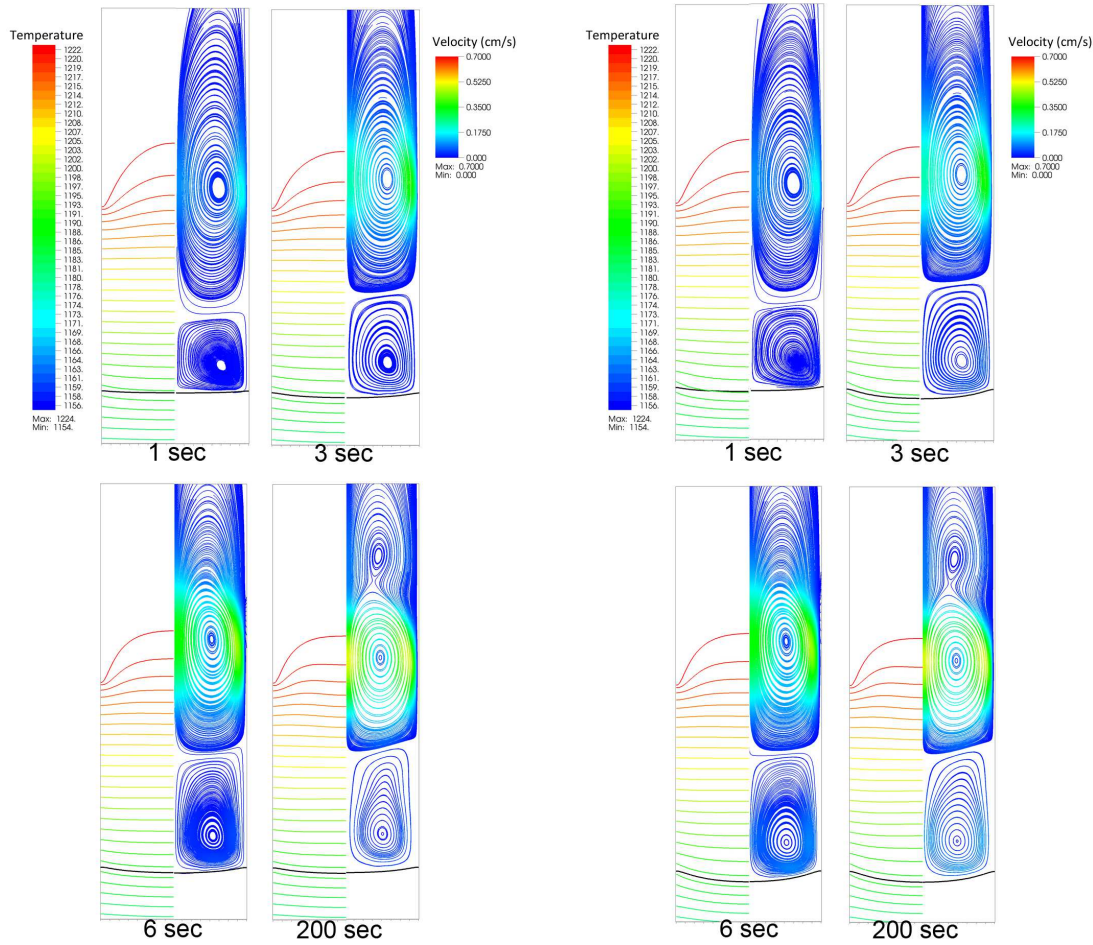| Dimensionless numbers	Expression	Characteristic values
Rayleigh number	$Ra=\frac{g\beta_T\Delta TL^3}{\mu\alpha_l}$	1.81×10^5
Prandtl number	$Pr=\mu/\alpha$	6.53×10^{-3}

Figure 5: Temperature distribution (left half side), streamline (right half side), and phase interface in vertical crystal growth system with pull speed $U_{pull} = 6.668 \times 10^{-6} m s^{-1}$ at 1, 3, 6, and 200 second.

Figure 6: Temperature distribution (left half side), streamline (right half side), and phase interface in vertical crystal growth system with pull speed $U_{pull} = 1.3336 \times 10^{-5} m s^{-1}$ at 1, 3, 6, and 200 second.

results shown in Fig. 5 and Fig. 6 are for the fixed wall temperature setup. If a time-dependent temperature profile setup is applied on the walls, the melt-solid interface will move up. Fig. 8 shows the comparison of phase interface shapes between two kinds of frame setups. The phase interface shapes are the same in the both cases, that means they are equivalent for the vertical gradient solidification system.

4.3 Effect of melt convection on crystal growth

In this section, the effect of convection in the melt region on the temperature distribution and crystal growth is studied. Fig. 9 shows the temperature distribution in the furnace
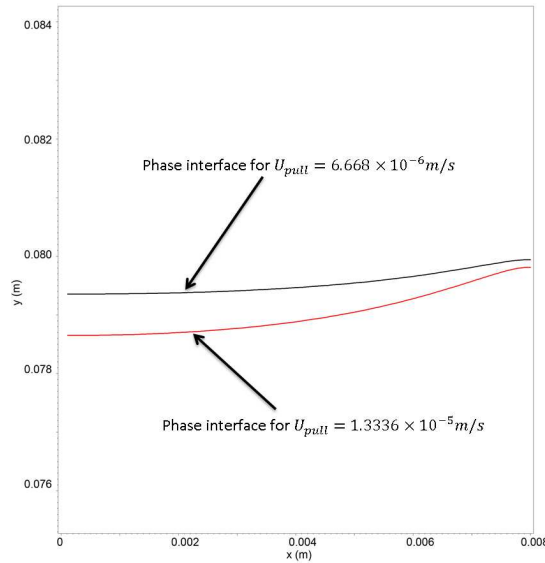
Figure 7: Comparison of phase interface shape between different pulling speeds in furnace.
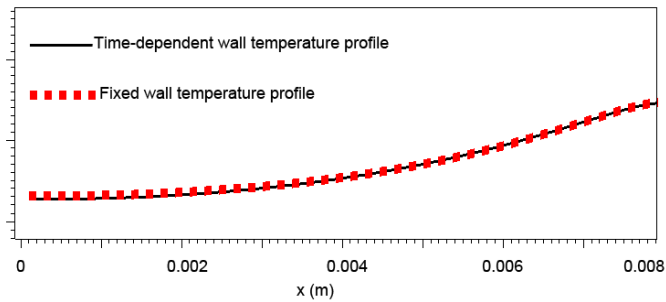

Figure 8: Comparison of phase interface shapes in the two different frame setups. Black line is from the fixed wall temperature profile setup, and red square is for the time-dependent temperature profile setup.

with and without considering the convection and turbulent fluid transport in the melt region. Generally, the effect of convection in the melt region is very limited, and the temperature distributions are almost the same in the both cases, especially near the phase interface. This means that the effect of convection is significantly suppressed, which meets the requirement of the vertical gradient crystal growth system. Fig. 10 shows the comparison of phase interface shapes between the case with and without convection. The convection makes the concave crystal surfaces a little bit less curvilinear. The convection helps take the latent heat during phase transition away from the phase interface, so the temperature is reduced a little near the interface, which causes the shape to be less curvilinear. Because the circulation is very weak, the temperature difference near the phase interface caused by the convection is small.
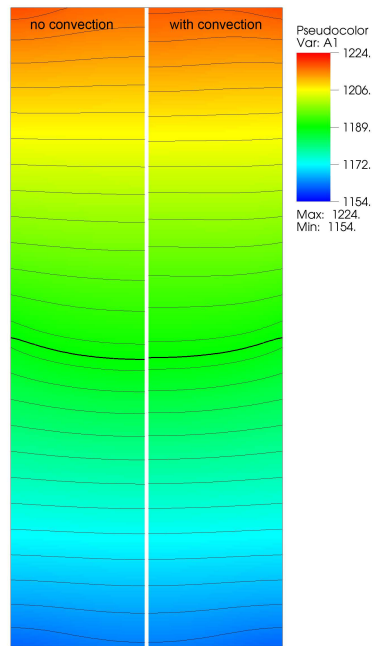
Figure 9: Temperature distribution in the furnace with and without considering the convection effects (left half side: no convection, right half side: with convection.
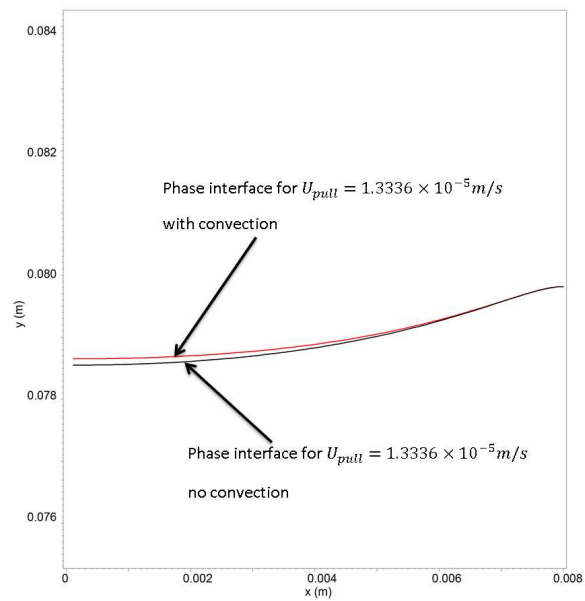

Figure 10: Comparison of phase interface shape between the case with and without considering convection effects.

4.4 Efficiency of the parallel computation

As mentioned in the previous section, a primary advantage of lattice-based CFD methods are their inherent parallelism [17, 23]. High Rayleigh number convection in melt region requires a small time step. Also, crystal growth is a very slow procedure, which often lasts several hours to a few days. The simulation of crystal growth is computation intensive when the Rayleigh number is high, especially for a 3-dimension simulation. In this section, we examine the efficiency of the parallel computation of the model. Fig. 11 shows the speedup for the program running on 10, 20, 40, and 80 CPU cores. The program shows considerable speedup with increasing the number of CPU cores. Because the tested cases are only 2-dimensional problems with only about 250 thousand lattices, performance of ParaFlow decreases for 80 or more cores. The performance can be improved by further program optimization and by applying the model to practical 3-dimensional problems.
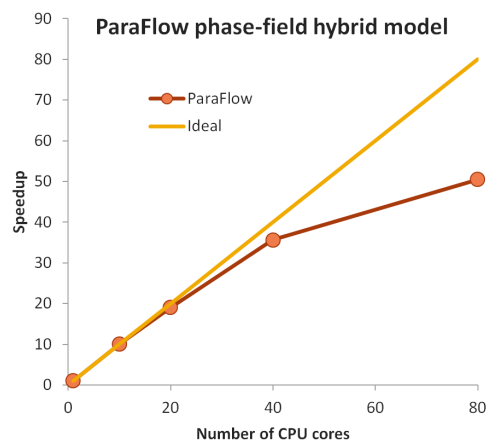

Figure 11: Speedup for the program running on 10, 20, 40, and 80 CPU cores.

5 Summary and discussion

A coupled lattice kinetics phase-field model for crystal growth in the vertical gradient furnace has been developed. The model takes into account buoyancy induced convective flow and its effect on the crystal growth process. Comparison of the phase-field model with an analytical solution for the macro-scale radial solidification shows the high accuracy of the phase-field approach in cases where capillary length is significantly smaller than the radius of the front curvature. This makes the phase-field applicable for the wide range of free-boundary problems including modeling of the macro-scale interface evolution during solidification in the vertical gradient furnace. A semi-implicit lattice kinetics method is used for solving the convection in the melt region. In the present work, the model was used to study the effect of the furnace operational conditions on crystal

growth. Because of the low computational cost on dealing with moving or transforming solid boundary conditions, two kinds of wall temperature profile setups can be applied in the proposed numerical model without efficiency difference. The simulation results shows the same melt-solid interface shape for these two kinds of setup, which proves that they are equivalent. Besides that, the wall temperature profile as shown in Eq. (2.4) can significantly suppress the effect of convection, especially near the melt-solid interface, which meets the requirement of the vertical gradient solidification system, and is favorable for high quality crystal growth. Finally, the parallel computation shows considerable speedup on the 2-dimension tests. It will be an efficient and powerful numerical simulation tool for further study in 3-dimension cases.

Acknowledgments

References

[1] M. Yildiz, S. Dost, B. Lent, Growth of bulk SiGe single crystals by liquid phase diffusion, J. Cryst. Growth 280 (1) (2005) 151–160.
[2] M. Yildiz, S. Dost, A continuum model for the liquid phase diffusion growth of bulk SiGe single crystals, International Journal of Engineering Science 43 (2005) 1059–1080.
[3] U. Becker, H. Zimmermann, P. Rudolph, R. Boyn, Optical study of the impurity distribution in vertical-Bridgman-grown CdTe crystals, Phys. Status Solidi (A) Applied Research 112 (2) (1989) 569–578.
[4] H. Hermon, M. Schieber, R. James, J. Lund, A. Antolak, D. Morse, N. Kolesnikov, Y. Ivanov, M. Goorsky, H. Yoon, J. Toney, T. Schlesinger, Homogeneity of CdZnTe detectors, Nuclear Instruments & Methods in Physics Research, Section A: Accelerators, Spectrometers, Detectors and Associated Equipment 458 (1) (2001) 100–106.
[5] H. Hermon, M. Schieber, E. Lee, J. McChesney, M. Goorsky, T. Lam, E. Meerson, H. Yao, J. Erickson, R. James, CZT detectors fabricated from horizontal and vertical Bridgman-grown crystals, Nuclear Instruments & Methods in Physics Research, Section A: Accelerators, Spectrometers, Detectors and Associated Equipment 410 (1) (1998) 503–510.
[6] P. Sonda, A. Yeckel, P. Daoutidis, J. J. Derby, Development of model-based control for Bridgman crystal growth, Journal of Crystal Growth 266 (1) (2004) 182–189.
[7] J. Derby, L. Lun, A. Yeckel, Strategies for the coupling of global and local crystal growth models, Journal of Crystal Growth 303 (1) (2004) 114–123.

[8] L. Lun, A. Yeckel, P. Daoutidis, J. Derby, Decreasing lateral segregation in cadmium zinc telluride via ampoule tilting during vertical Bridgman growth, Journal of Crystal Growth 291 (2) (2006) 348–357.

[9] P. Sonda, A. Yeckel, J. Derby, P. Daoutidis, The feedback control of the vertical Bridgman crystal growth process by crucible rotation: two case studies, Computers and Chemical Engineering 29 (2005) 887–896.

[10] P. Sonda, A. Yeckel, P. Daoutidis, J. Derby, Hopf bifurcation and solution multiplicity in a model for destabilized Bridgman crystal growth, Chem. Eng. Sci. 60 (2005) 1323–1336.

[11] A. Pandy, A. Yeckel, M. Reed, C. Szeles, M. Hainke, G. Mller, J. Derby, Analysis of the growth of cadmium zinc telluride in an electrodynamic gradient freeze furnace via a self-consistent, multi-scale numerical model, Computers and Chemical Engineering 276 (2005) 133–147.

[12] T. Nishinaga, Microchannel epitaxy: an overview, J. Cryst. Growth 237 (2002) 1410–1417.

[13] Y. Liu, Z. Zytkiewicz, S. Dost, A model for epitaxial lateral overgrowth of GaAs by liquid phase electroepitaxy, J. Cryst. Growth 265 (4) (2004) 341–350.

[14] G. Fix, Free Boundary Problems: Theory and Applications, Piman, Boston, 1983.

[15] A. Karma, W.-J. Rappel, Quantitative phase-field modeling of dendritic growth in two and three dimensions, Physical review E 57 (4) (1998) 4323–4349.

[16] B. Echebarria, R. Folch, A. Karma, M. Plapp, Quantitative phase-field model of alloy solidification, Physical Review E 70 (2004) 0616041–06160422.

[17] D. Rector, M. Stewart, A semi-implicit lattice method for simulating flow, J. Comp. Phys. 229 (2010) 6732–6743.

[18] R. Benzi, S. Succi, M. Vergassola, The lattice Boltzmann equation: theory and applications, Phys. Rep. 222 (1992) 145.

[19] S. Chen, G. Doolen, Lattice Boltzmann method for fluid flows, Ann. Rev. Fluid Mech. 30 (1998) 329–364.

[20] D. Yu, R. Mei, L. Luo, W. Shyy, Viscous flow commutations with the method of lattice Boltzmann equation, Progr. Aerosp. Sci 39 (2003) 329–367.

[21] S. Succi, The Lattice Boltzmann Equation for Fluid Dynamics And Beyond, Oxford University Press, Oxford, 2001.

[22] T. Inamuro, A lattice kinetic scheme for incompressible viscous flows with heat transfer, Philos. T. Roy. Soc. A 360 (2002) 477–484.

[23] D. Rector, M. Stewart, J. Bao, Modeling of HLW tank solid resuspension and mixing process, WM2102 Conference, Phoenix, AZ, 2012.

[24] X. He, L. Luo, A priori derivation of the lattice Boltzmann equation, Phys. Rev. E 55 (1997) R6333–R6336.

[25] H. Lee, A. Pearlstein, Simulation of radial dopant segregation in vertical Bridgman growth of GaSe, a semiconductor with anisotropic solid-phase thermal conductivity, J. Crystal Growth 231 (2001) 148–170.

[26] H. Lee, A. Pearlstein, Simulation of vertical Bridgman growth of benzene, a material with anisotropic solid-phase thermal conductivity, J. Crystal Growth 209 (2000) 934–952.

[27] A. Karma, Phase-Field formulation for quantitative modeling of alloy solidification, Phys. Rev. Lett. 87 (2001) 115701–115705.

[28] Z. Guo, C. Zheng, B. Shi, Discrete lattice effects on the forcing term in the lattice Boltzmann method, Phys. Rev. E 65 (2002) 046308–046314.

[29] X. He, L. Luo, Lattice Boltzmann model for the incompressible Navier-Stokes equation, J. Stat. Phys. 88 (1997) 927–944.

[30] D. Wolf-Gladrow, Lattice-gas cellular automata and lattice Boltzmann models: an introduc-

tion. Lecture Notes in Mathematics, Vol. 1725, Springer, 2000.

[31] C. Aidun, Y. Lu, Lattice Boltzmann simualtions of solid particles suspended in fluid, J. Stat. Phys 81 (1995) 49–61.

[32] A. Ladd, Numerical simualtions of particulate suspensions via a discretized Boltzmann equation, J. Fluid Mech 271 (1994) 285–339.

[33] D. Ziegler, Boundary conditions for lattice Boltzmann simulations, J. Stat. Phys. 71 (1993) 1171–1177.

[34] O. Filippova, D. Hanel, Grid refinement for lattice-BGK models, J. Comp. Phys. 147 (1998) 219–228.

[35] J. Bao, P. Yuan, L. Schaefer, A mass conserving boundary condition for the lattice Boltzmann equation method, J. Comp. Phys. 227 (2008) 8472–8487.

[36] H. Carslaw, J. Jaeger, Conduction of Heat in Solids, Oxford University Press, 1959.

[37] O. Filippova, S. Succi, F. Mazzocco, C. Arrighetti, G. Bella, D. Hanel, Multiscale lattice Boltzmann schemes with turbulence modeling, J. Comput. Phys. 170 (2001) 812–829.